Supplementary information

Silver quasi-nanoparticles: bridging the gap between clusters molecular-like and plasmonic nanoparticles

Fatima Douma[a], Louwanda lakiss[a], Oleg I. Lebedev[b], Julien Cardin[c], Krassimir L. Kostov[d], Jaafar El Fallah[a], Valentin Valtchev[a] and Mohamad El-Roz[a]*

1. Optimization of ZX-Bi synthesis

1.1. Effect of the aging time

The aging time corresponds to the duration after the mixing of the solutions A and B used in the preparation of the zeolite (please see the experimental section). Despite that this factor has no significant impact on the synthesis of the parent zeolite (ZX), an important effect is observed in the case of the ZX-Bi. The X-ray diffractograms of the ZX-Bi-3 samples prepared, with similar conditions, after 24 h (traditional time used for ZX) and 14 h of aging time are presented in figure S1. The results indicate that the sodalite phase is promoted by increasing the aging time. This inspected effect of the aging time can probably be related to the nucleation process of faujasite probably accelerated with the presence of Bi cations in the synthesis medium.

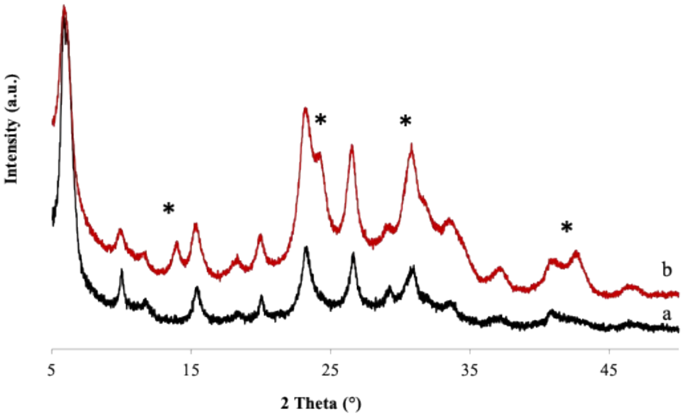

Fig. S1. X-ray patterns of the ZX-Bi-3 samples crystallized at 50 °C for 24h after (a) 8 h and (b) 14h of aging time at room temperature (RT). Peaks labeled with stars correspond to the sodalite phase.

I.2. Effect of water content

It is well known that zeolite crystallization might also be affected by the initial concentration of water in the synthesis media [1]. The amount of water added to the synthesis mixture for faujasite crystallization found to be very critical (Figure S2). A high dehydration (> 50%) of the solution (after the aging) can promote the formation of sodalite and affect the crystallinity, respectively. Such an effect is less significant in case of the preparation of the parent FAUX or even for the ZX-V sample under the same conditions. The optimal rates of dehydration are around 40±5% (corresponds to the amount of the water eliminated by freeze drying in respect to the total amount of water added to the initial gel).

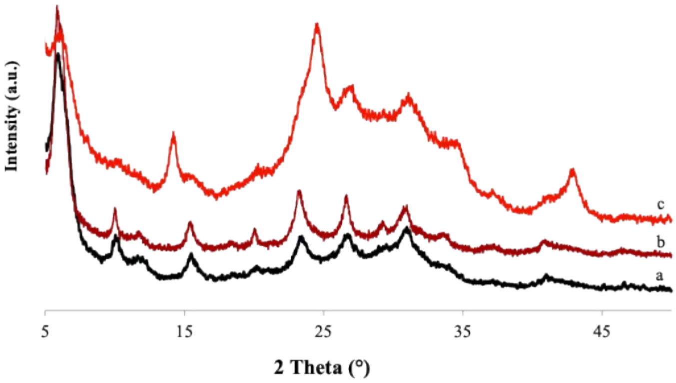

Fig. S2. X-ray patterns of ZX-Bi-3 samples prepared after an aging time of 14h followed by dehydration by freeze drying, of the following water ratio: 30%, 40%, and 50%, respectively. All the samples are crystallized for 8 h at 50 °C.

I.3. Crystallization time effect

After fixing the aging time to 14h, the duration of the hydrothermal synthesis is optimized in order to enhance the sample crystallinity. The temperature is always fixed at 50°C to preserve the nanosize of the zeolite particles. Figure S4 shows the evolution of the X-ray diffraction patterns of zeolite ZX-Bi-3 with the crystallization times. After 2 hour of crystallization, broad reflection peaks of zeolite FAU can be detected. This indicates that amorphous compounds are still present. However, extending the heating time up to 14-24 hours favors a phase transition into sodalite type zeolite. Indeed, sodalite appears after heating for 14 hours. An optimal crystallinity was observed between 5 to 7 hours of crystallization (versus 24-48h for ZX).

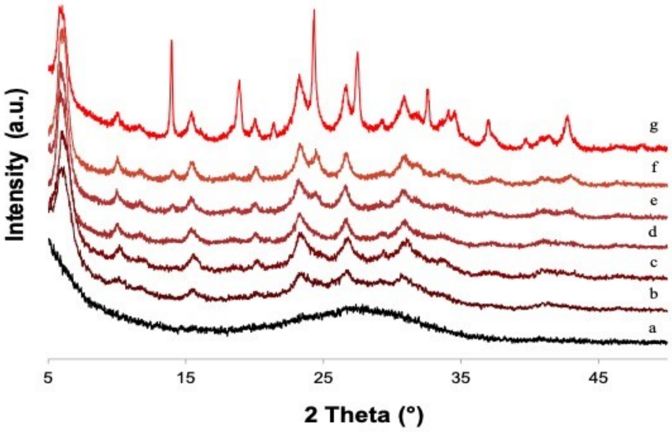

Fig. S3. X-ray diffractograms of ZX-Bi-3 prepared after 14h of aging followed by a crystallization at 50 °C during: (a) 0h, (b) 2h, (c) 5h, (d) 7h, (e) 14h, (f) 24h, and (g) 48h.

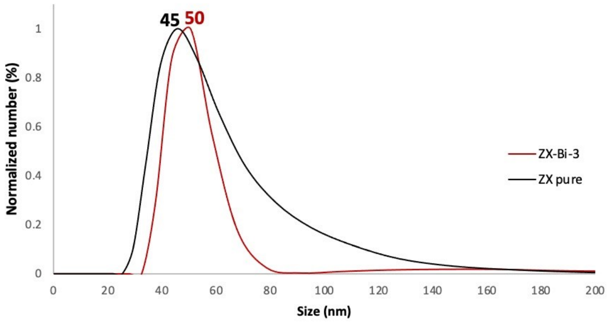

Fig. S4. The DLS results of (a) pure ZX and (b) ZX-Bi-3 crystallized for 24h and 8h respectively. Crystallization temperature: 50 °C; aging for 14 and 24h at RT respectively.

2. General Characterization of ZX-Bi and Ag@ZX-Bi-X

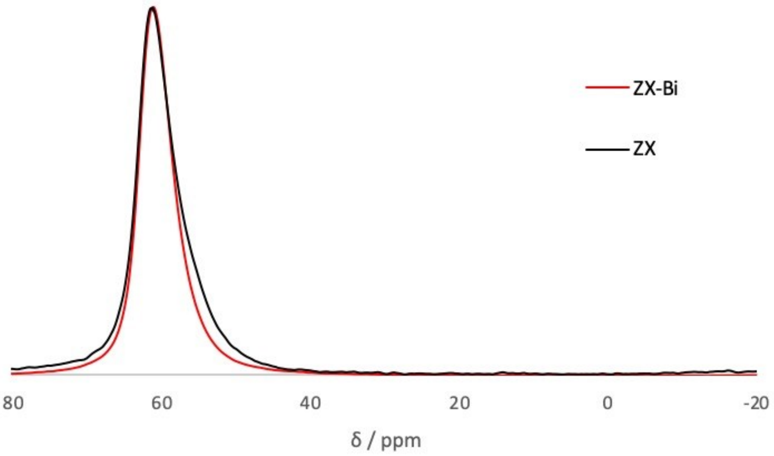

Fig. S5. 27 Al MAS NMR spectra of the hydrated samples ZX and ZX-Bi samples.

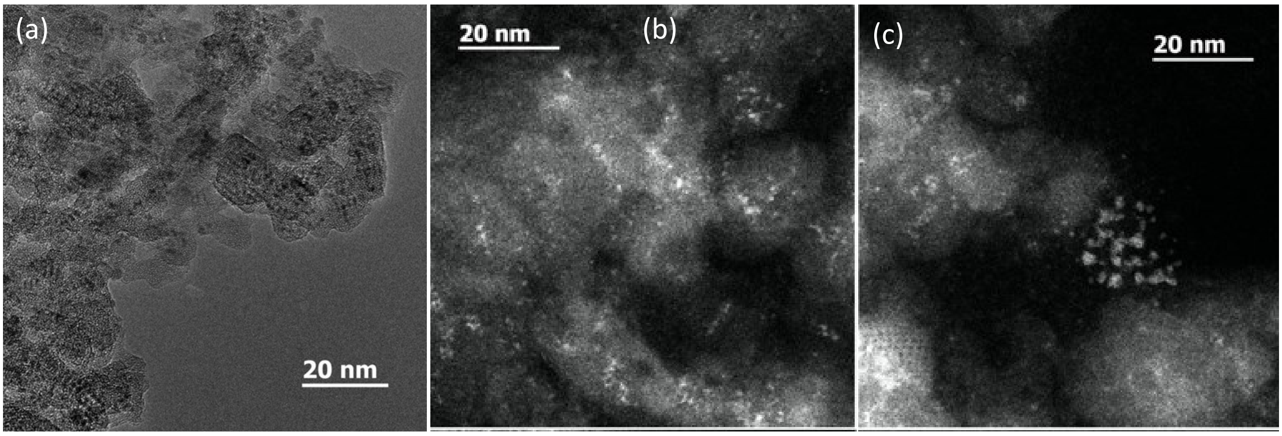

Fig. S6. (a) Bright field low magnification TEM and (b-c) HAADF-STEM analysis of the ZX-Bi sample, dark and bright dots correspond to Bi species, respectively.

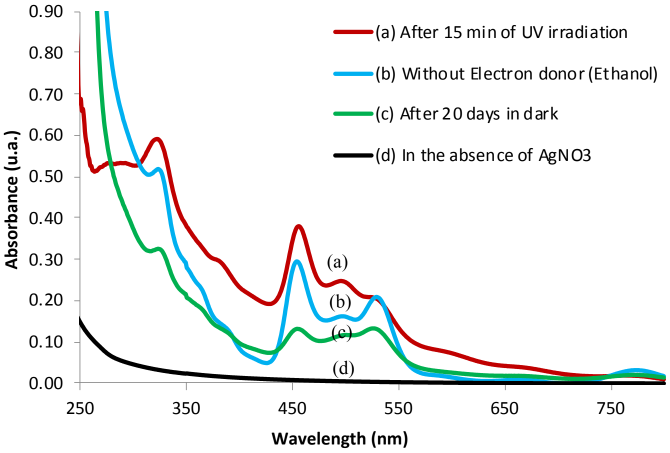

Fig. S7. Evolution of the UV-visible absorbance spectrum of (a) The irradiated ZX-Bi (*) in the absence of $AgNO_3$, (b) ZX-Bi suspension irradiated for 15 min in the presence of $AgNO_3$ without adding ethanol (c) ZX-Bi in water/ethanol (3/1) in the presence of $AgNO_3$ after one month of exposure to visible light and without UV irradiation, (b) ZX-Bi in water/ethanol (3/1) in the presence of $AgNO_3$ and irradiated for 15 min. Conditions: Hg-Xe lamp; polychromatic irradiance = 205 mW / cm^2; infrared cut filter; total volume = 5 ml; $[AgNO_3] = 10^{-2}$; [ZX-Bi3%] = 2.4 g / l. (*): (a) Spectrum not subtracted from the sample before irradiation.

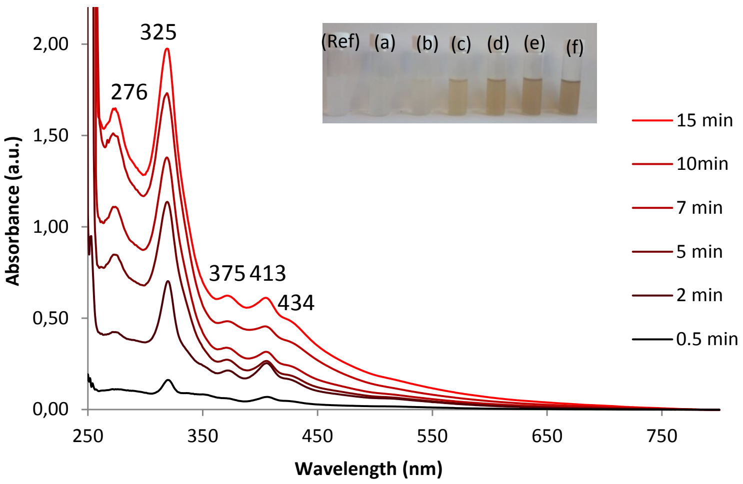

Fig. S8. Time evolution of UV-vis absorption spectra of ZX-V suspensions after (a) 0.5, (b) 2, (c) 5 (d) 7, (e) 10 et (f) 15 min of UV irradiation in presence of 10-2 M of $AgNO_3$. (Ref) correspond to the sample before irradiation. Conditions: lamp Hg-Xe; polychromatic = 205 mW/cm^2; filter cut infrared; total volume = 5 ml; $[AgNO_3] = 10^{-2}$; [ZX-Bi] = 2.4 g/l. Inset: Optical images of the corresponding suspensions.

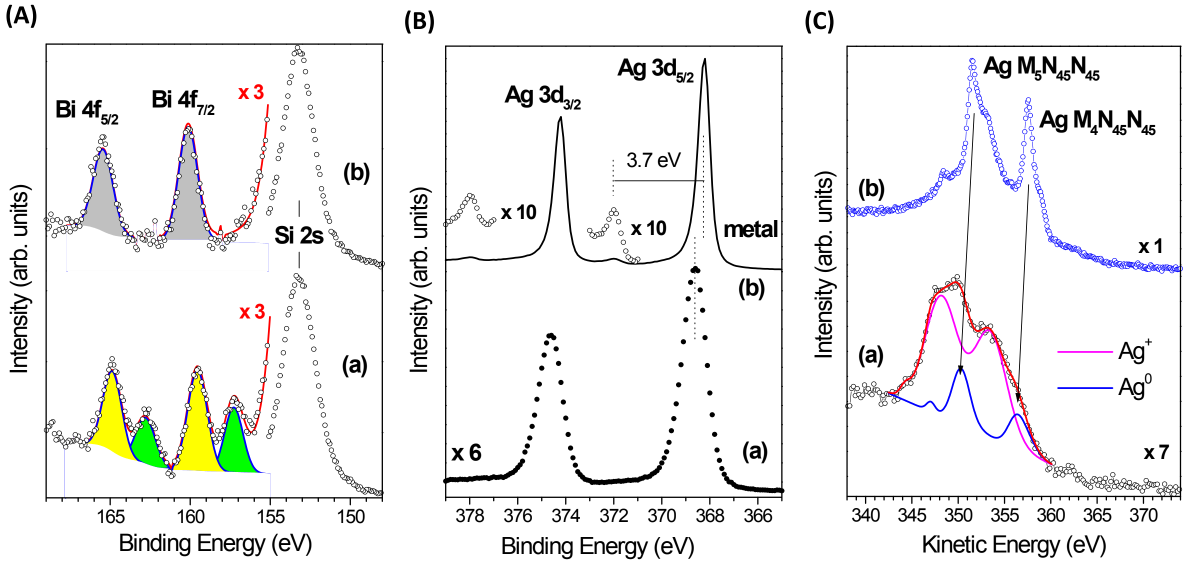

Fig. S9. A) Gaussian deconvolutions of the XPS spectra of ZX-Bi-3 (a) and Ag@ZX-Bi-3 (b) samples. The red lines correspond to the intensity sum of the different peak contributions. B) Comparison of the Ag 3d photoelectron regions of Ag@ZX-Bi (a) and metal Ag foil (b). C) Comparison between Ag MNN spectra of Ag@ZX-Bi (a) and metal Ag folio (b).

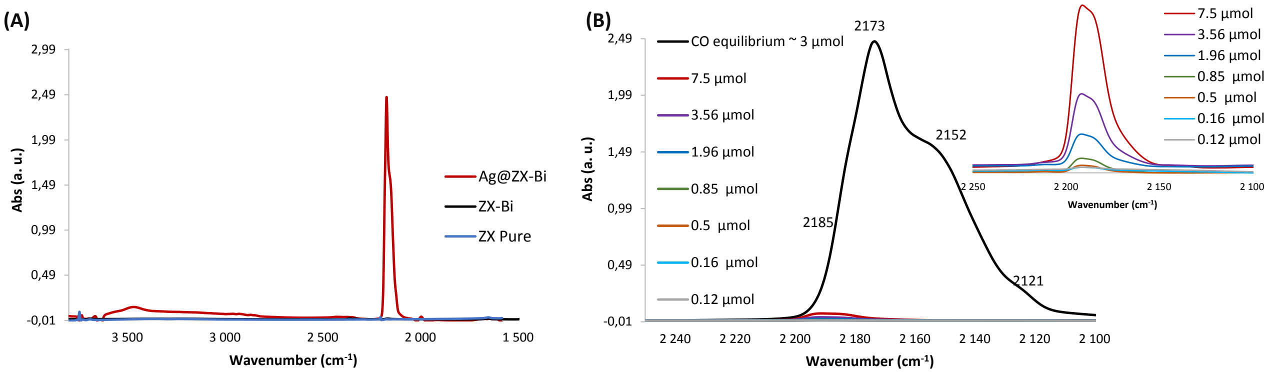

Fig. S10. (A) IR spectra of ZX, ZX-Bi and Ag@ZX-Bi at equilibrium under 20 torr of CO. The spectra are subtracted from the spectra of the activated samples under vacuum (before CO adsorption). (B) Evolution of the band intensities of adsorbed CO on Ag@ ZX-Bi at 77 K (the sample was activated at 200°C under vacuum over the night), Insert: zoom of the IR spectra for small pressures of CO. For ZX pure and ZX-Bi the typical bands of carbonyl groups are not depicted, while an intense band at 2173 cm^{-1} is observed after CO adsorption on Ag@ZX-Bi (Figure S11). The shoulder at 2185 and the strong peak at 2173 cm^{-1} are attributed to the monocarbonyl Ag^{+}(CO) due to the presence of different electron acceptor sites of Ag^{+} inside the zeolite structure. However, the bands at 2152 and 2121 cm^{-1} are characteristic of the formation of Ag$_{n}^{0}$-CO complexes [2, 3, 4]

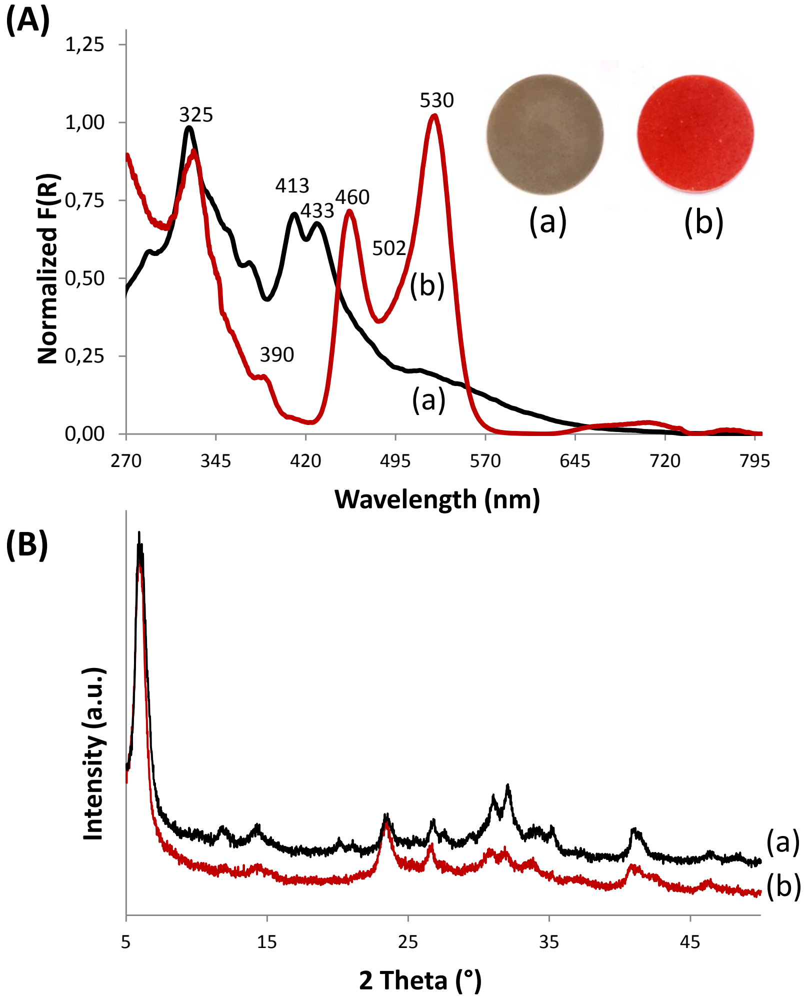

Fig. S11. (A) DR-UV-visible spectra and (B) X-ray diffractograms of Ag@ZX-V (a) and Ag@ZX-Bi (b) powders. Inset A: pellet form of Ag@ZX-V and Ag@ZX-Bi (diameters: 2 cm^2, thickness: 65 µm).

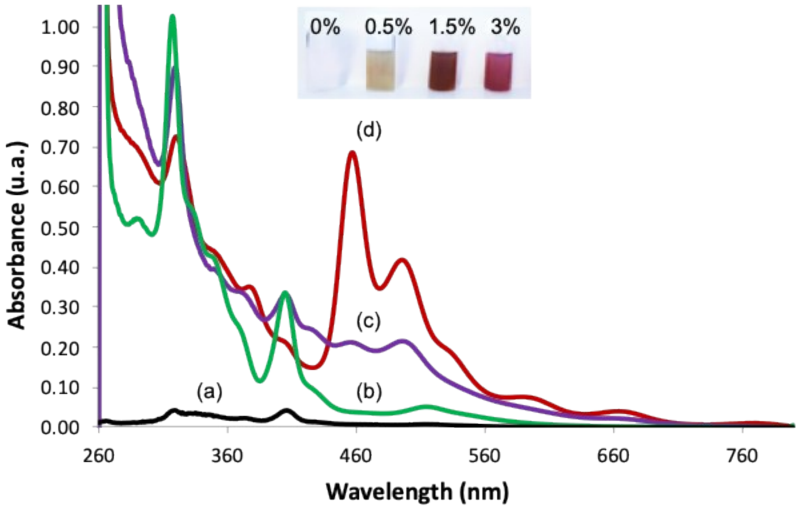

Fig. S12. Evolution of the UV-visible absorbance spectrum of (a) ZX, (b) ZX-Bi-0.5, (c) ZX-Bi-1.5, (d) ZX-Bi-3 suspensions after 15 min of irradiation under UV in presence of excess of sliver nitrate. Conditions: Hg-Xe lamp; polychromatic irradiance = 205 mW / cm^2; infrared cut filter; total volume = 5 ml; [$AgNO_3$] = 10^{-2}M; [zeolite] = 2.4 g / l. (*): all spectra are subtracted from the spectrum of the corresponding samples before irradiation.

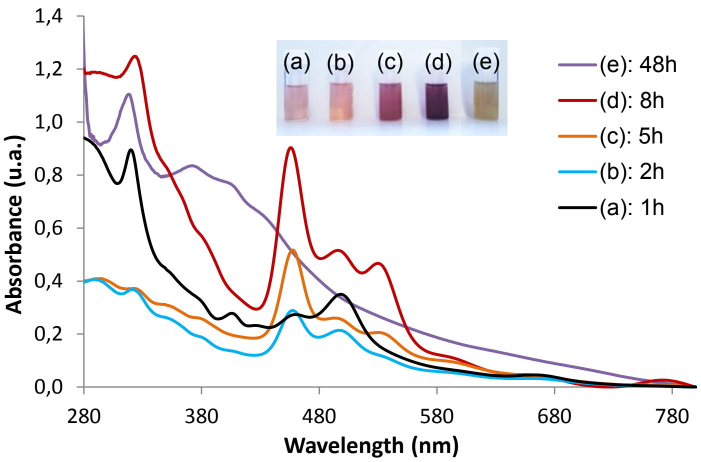

Fig. S13. UV-Visible spectra of the material suspensions, crystallized for different crystallization times, after 15 of UV irradiated in presence of excess of silver nitrate. All samples are prepared in similar condition than that used for ZX-Bi-3 except the crystallization time (please refers to the experimental section and the main text for more details about the synthesis). The XDR patterns of the corresponding samples are reported in Figure S4. The ICP analyses are reported in table S1. Insert: images of the corresponding suspensions

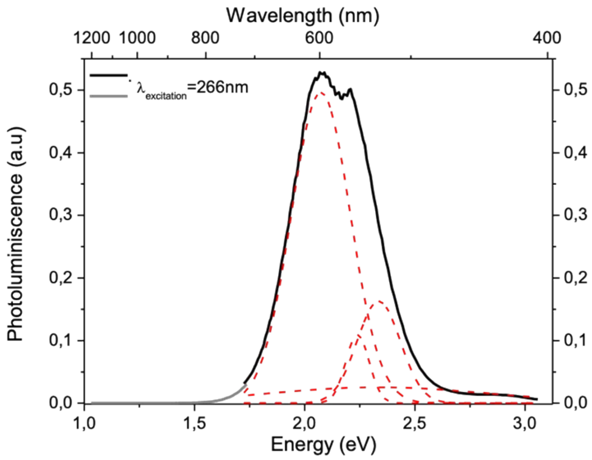

Fig. S14. PL spectra of Ag@ZX-V sample. Excitation laser wavelength is either 266 nm (black&grey) or at 488 nm (blue). PL bands were fitted by means of Gaussian function (doted red lines). Long pass filters were used with the cut-on wavelength at 700 nm for grey and blue curves.

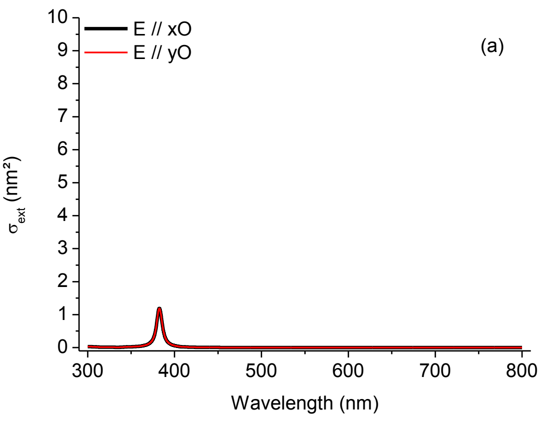

Fig. S15. Extinction cross-section of single silver nanostructure with 1nm of size.

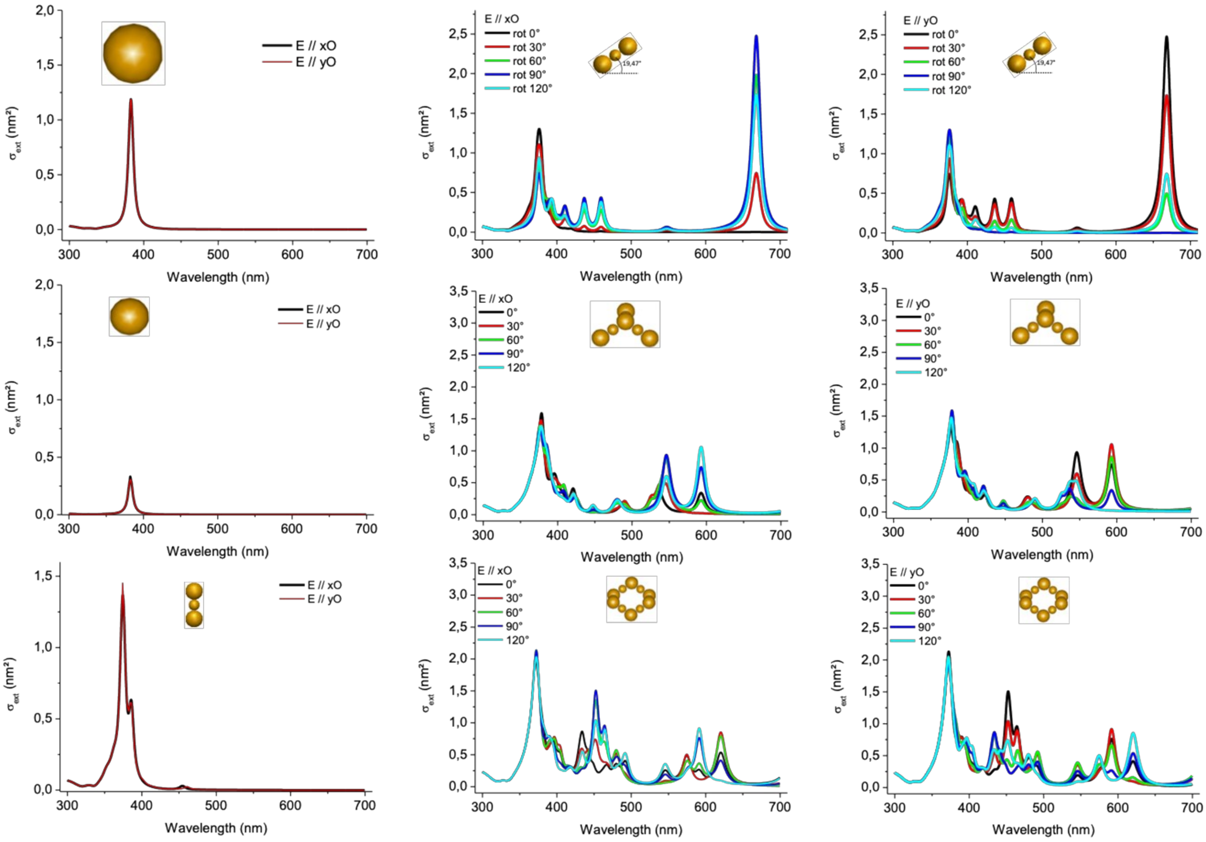

Fig. S16. Evolution of the extinction cross-section of silver nanostructures with isolated and interconnected nanoparticles with different polarization angle along xO and yO axis.

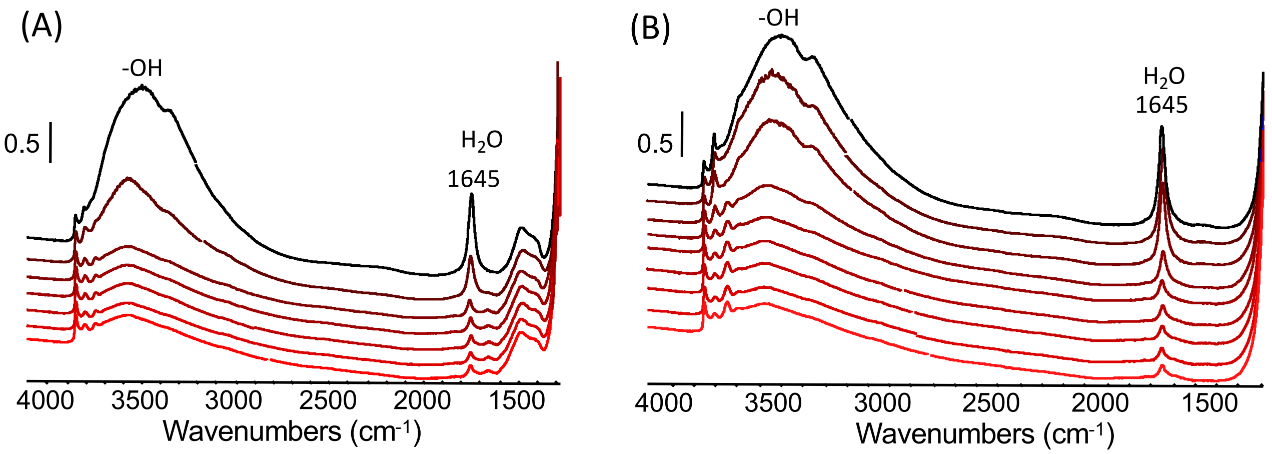

Fig. S17. Evolution of the IR spectra of (A) Ag@ZX-Bi and (B) Ag@ZX-V under first minute of visible light irradiation under Ar. Resolution: 2 min/spectrum. The results show a 2 to 3 times faster desorption of water under similar irradiation conditions.

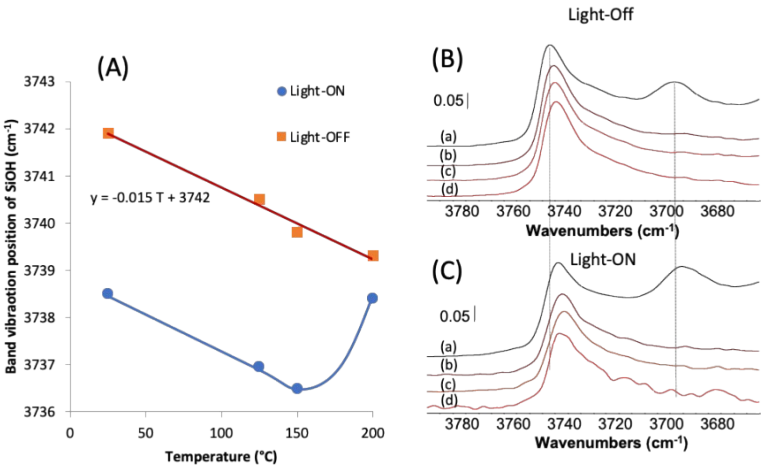

Fig. S18. (A) Evolution of the vibration band position of the isolated SiOH in the Ag@ZX-Bi sample versus the temperature in dark (square) and under visible irradiation (circle). Figures (B) and (C) display the corresponding IR spectra, respectively, at 25 (a), 120 (b), 150 (c) and 200 °C (d) in the vibration range of isolated SiOH.

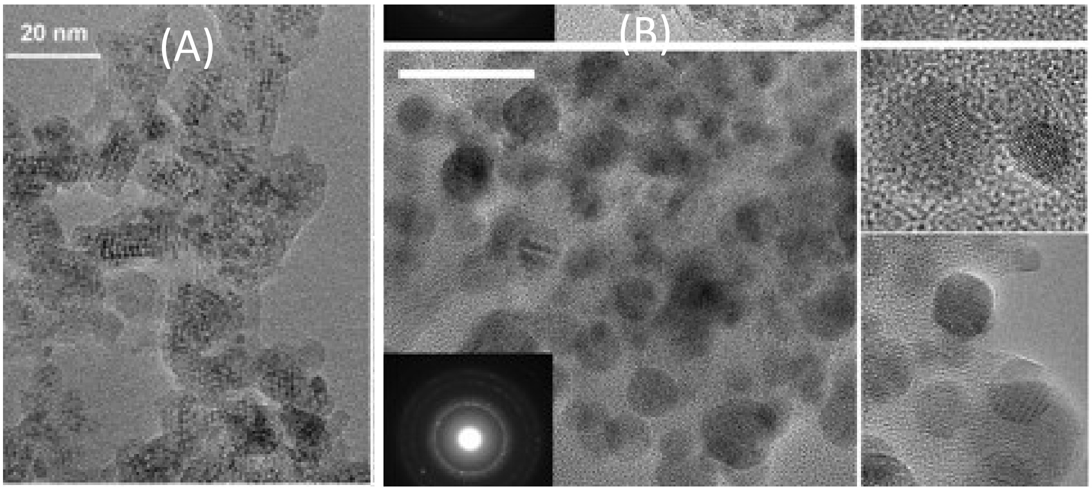

Fig. S19. HR-TEM images of Ag@ZX-Bi before (A) and after (B) activation at 200°C under Ar. The dark spots correspond to the silver particles and a migration of the quasi-NPs Ag and aggregation on the surface to form AgNPs (≈5nm) can be observed after activation.

Tables

Table S1: Crystallinity of the prepared samples after 14h of aging followed by a crystallization at 50°C for different duration.

Sample (time of the crystallization)	Crystallinity*%	FAU:SOD %:%
ZX-Bi-3 (0h)	0%	/
ZX-Bi-3 (2h)	25.85%	>99% FAU
ZX-Bi-3 (5h)	35.26%	>99% FAU
ZX-Bi-3 (8h)	98%	>99% FAU
ZX-Bi-3 (14h)	56%	68% FAU 32 SOD
ZX-Bi-3 (24h)	62%	65% FAU 35% SOD
ZX-Bi-3 (48h)	/%	43.5% FAU 56.5% SOD

* The crystallinity of zeolite samples is estimated using a pure ZX sample is used as a reference. Then the crystallinity of the as-synthesized samples was estimated by comparing the integrated area of the reflection peaks of ZX-Bi relatively to their corresponding peaks in the pure ZX (at 2θ= 20.25, 23.48 and 26.82°)

Table S2. The elemental composition of ZX-Bi samples as determined by ICP and EDX (between brackets) analysis.

Samples	Si/Al	Bi atm.% (wt.%)	Na atm.% (wt.%)
ZX-Bi-3	1.27	0.74 (2.3)	27(22)
ZX-Bi-1.5	1.41	0.33 (1.15)	27(23)
ZX-Bi-0.5	1.44	0.18 (0.38)	28 (23)

Table S3. Assignment of the different absorbance bands of AgCLs as reported in the literature.

Absorbance	Attributions	References
266-310 nm	$Ag_n^{\delta+}$ cluster eg. Ag_3^+, Ag_4^{2+}, ionic $Ag_8^{\delta+}$	[5, 6]
The two shoulders at around 295 and 355 nm	Ag_4^{2+}	[7, 8]
325 nm	the atomic Ag_8^0 in the sodalite cavities	[9]
380 nm	Ag species containing approximately seven nuclei	[10, 11]
407 nm	larger ionic cluster	[11]
458, 500 and 540 nm	the strong interaction of the zeolite ligand and the silver clusters by a transitional charge transfer (LMCT).	[12, 13]
597 and 670 nm	electron tunneling effect (electron transfer between the clusters)	[6]

Tables S4. Bi/Al ratio, Bi content (ICP results) and crystallinity of Bismuth containing FAU zeolite samples crystallized at different times.

Crystallization time	Si/Al	Bi (wt.%)	Crystallinity % and composition (FAUX: SOD)
1h	1.37	2.17	13% (>99% FAU:<1% SOD)
2h	1.27	2.3	25% (>99% FAU:<1% SOD)
5h	1.24	2.3	35 (>99% FAU:<1% SOD)
8h	1.55	2.4	>95% (99%FAUX/1%SOD)
48h	1.47	2.3	>95%(48%FAUX/51%SOD)

References

---

[1] J. Grand, H. Awala, & S. Mintova, *CrystEngComm*, 2016, ***18***, 650-664.
[2] K. I. Hadjiivanov, & G. N. Vayssilov, Advances in Catalysis, 2002, ***49***, 307-511.
[3] K. Góra-Marek, K. A. Tarach, Z. Piwowarska, M. Łaniecki, & L. Chmielarz, *Catalysis Science & Technology*, 2016, **6(6)**, 1651-1660.
[4] H. I. Hamoud, M. Lafjah, F. Douma, O. I. Lebedev, F. Djafri, V. Valchev, M. El-Roz, *Solar Energy*, 2019, **189**, 244-253
[5] . Tuzovskaya, N. Bogdanchikova, A. Pestryakov, V. Gurin, A. Simakov, & V. Lunin, *Advances in the Understanding and Application of Catalysts*. 2003, **248**.

[6] V. S. Gurin, N. E. Bogdanchikova, V. P. Petranovskii, *The Journal of Physical Chemistry B*. 2000, **104**, 12105-12110.
[7] T. Yumura, A. Oda, H. Torigoe, A. Itadani, Y. Kuroda, T. Wakasugi, H. Kobayashi, *The Journal of Physical Chemistry C*, 2014, **118**, 23874-23887.
[8] E. Fron, S. Aghakhani, W. Baekelant, D. Grandjean, E. Coutino-Gonzalez, M. Van der Auweraer, J. Hofkens, The Journal of Physical Chemistry C, 2019, **123**, 10630-10638.
[9] B. Concepción-Rosabal, G. Rodríguez-Fuentes, N. Bogdanchikova, P. Bosch, M. Avalos, V. H. Lara, *Microporous and Mesoporous Materials*, 2005, **86**, 249-255.
[10] R. Kellerman, J. Texter, *The Journal of Chemical Physics*. 1979, **70**, 1562-1563.
[11] E. Gachard, J. Belloni, M. A. Subramanian, *Journal of Materials Chemistry*, 1996, **6**, 867-870.
[12] S. Aghakhani, D. Grandjean, W. Baekelant, E. Coutiño-Gonzalez, E. Fron., K. Kvashnina, P. Lievens, *Nanoscale*, 2018, **10**, 11467-11476.
[13] R. Seifert, R. Rytz, G. Calzaferri, *The Journal of Physical Chemistry A*, 2000, **104(32)**, 7473-7483.